Exploring micro-scale heterogeneity as a driver of biogeochemical transformations and gas transport in peat

Lukas Kohl[1,2,3], Petri Kiuru[4], Marjo Palviainen[5], Maarit Raivonen[1], Markku Koskinen[2,6], Mari Pihlatie[2,6], and Annamari Laurén[4,5]

[1]Institute for Atmospheric and Earth System Research (INAR)/Physics, Faculty of Science, University of Helsinki, Helsinki, Finland
[2]University of Helsinki, Faculty of Agricultural Sciences, Department of Agricultural Sciences, Helsinki, Finland
[3]Department of Environmental and Biological Sciences, Faculty of Science, Forestry and Technology, University of Eastern Finland, Kuopio, Finland
[4]School of Forest Sciences, Faculty of Science, Forestry and Technology, University of Eastern Finland, Joensuu, Finland
[5]Department of Forest Sciences, University of Helsinki, Helsinki, Finland
[6]Institute for Atmospheric and Earth System Research (INAR)/Forest Sciences, Faculty of Agriculture and Forestry, University of Helsinki, Helsinki, Finland

Correspondence: Lukas Kohl (lukas.kohl@helsinki.fi)

Abstract. Peat pore network architecture is a key determinant of water retention and gas transport properties, and has therefore been hypothesized to control redox conditions in and greenhouse gas emissions from peat soils. Yet, experimental ~~proof of the impact of the pore network structure on biogeochemical reactions remains~~ approaches to directly visualize the spatial heterogeneity of biogeochemical reactions in pore networks remain scarce. Here, we report on a ^{13}C pulse-chase assay developed to functionally explain and visualize the cm-scale heterogeneity in greenhouse gas emissions in peat cores. We injected a ^{13}C labeled substrate ($^{13}C_2$-acetate) at ~~different depths in the peat cores~~ 2 to 8 cm depths and monitored its conversion into CO_2 and CH_4 ~~and the subsequent transport to the core headspace~~. We then measured the pore network architecture of the same cores by X-ray microtomographic imaging and constructed the air-filled pore networks using pore network modeling. We ~~found~~ applied this approach to peat cores collected at a drained peatland forest in Southern Finland in an experiment to study the effects of water hysteresis, i.e., differences between peat cores that reached a given water potential (-20 hPa) from dryer or wetter conditions. We find large heterogeneity among the replicate cores and injections, indicating the effects of cm-scale heterogeneity on biochemical processes and gas transport. ~~This heterogeneity was largely present at the core (10 cm~~ These treatments resulted in similar average air-filled porosity, but distinct pore networks (higher coordination numbers and clustering coefficients in drying compared to wetting soils) and within-core ~~(cm) scale heterogeneity whereas little additional variance occurred on the stand (>10m) scale. Deeper injections resulted in a smaller faction of the label being converted to~~ water distribution. Substrate injection experiments revealed less (potential) microbial activity (less of the substrate emitted as CO_2) at grater depth in both treatments. In peat cores from the drying treatment we also find longer slower microbial response to label additions greater depths (slower release of label-derived CO_2 ~~and this fraction being emitted more slowly from the peat cores. Greater peat~~), while the timing of emissions did not vary in wetting treatments. Peat air-filled porosity was and pore network metrics could not explain the fraction of label converted to CO_2, but greater porosity ~~as well as~~ was associated

with slower CO_2 emissions whereas higher clustering coefficients and betweenness centrality (two measures of pore network properties) were associated with ~~slower~~ faster emissions.

Copyright statement. TEXT

1 Introduction

25 Peat pore network architecture controls microscale gas exchange, which determines redox conditions, the production of the greenhouses gases carbon dioxide (CO_2) and methane (CH_4), and their transport by diffusion and ebullition ~~(Kiuru et al., 2022b; Ramirez e~~ (Ramirez et al., 2016; Kiuru et al., 2022b). Yet, empirical methods that explain and visualize the role of pore networks and small-scale heterogeneity in the regulation of soil functions remain elusive. This is especially the case for peat soils, which possess complex pore structures distinct from mineral soils and which remain understudied compared mineral agricultural soils

30 (McCarter et al., 2020).

Peatlands are of global importance as modulators of biogeochemical cycles and greenhouse gas balances (Gorham, 1991; Limpens et al., 2008). Globally, more than 600 Gt of C are stored in peat layers (Yu et al., 2008), which are sensitive to drainage, forest management, and changes in environmental conditions. In a warming climate, peatlands are becoming a major source of greenhouse gases (GHG) such as CO_2 and CH_4 (Leifeld et al., 2019; Frolking et al., 2011). In peat, the production of

35 CO_2 and CH_4 are primarily determined by soil temperature and oxygen (O_2) supply (McCarter et al., 2020). Where sufficient O_2 is available, heterotrophic respiration dominates and peat is decomposed to CO_2. In the absence of O_2, peat decomposition uses other electron acceptors, which eventually leads to methanogenesis. This occurs, for example, below the water table (WT) and above the WT in ~~aerobic~~ anaerobic microsites (anaerobic pockets) (Wachinger et al., 2000; Hagedorn et al., 2011). At this ~~micro-scale~~microscale, O_2 concentrations depend on the balance between O_2 consumption, driven by temperature and

40 substrate availability, and on the O_2 transport from the atmosphere to soil (McCarter et al., 2020; Keiluweit et al., 2018). This transport, in turn, depends on the peat water content and the connectivity and structure of the air-filled macropore network in the peat ~~(Kiuru et al., 2022a, b)~~(King and Smith, 1987; Boon et al., 2013; Hamamoto et al., 2016; Kiuru et al., 2022b). Small-scale heterogeneity in the pore structure may explain the noisy and peaky patterns of methane emissions typically observed in field conditions ~~(Xu et al., 2016)~~(Xu et al., 2016; Wright et al., 2018).

45 ~~Air-filled macropores in peat can be identified by microtomographic imaging that are abstracted into pore network models (PNM) (Kettridge and Binley, 2011; Rezanezhad et al., 2016; Kiuru et al., 2022a, b). This approach allows simulation of physical processes, such as water retention (Kiuru et al., 2022a) and gas transport (Kiuru et al., 2022b). Pore networks can also be analysed based on network metrics (Newman, 2006), and pore network imaging can help in identifying macropores that are isolated from the larger pore network and from the atmosphere (Kiuru et al., 2022a). PNM has suggested that the proportion~~

50 ~~of such isolated pores decreases with decreasing water content, and that hysteretic behaviour of soil wetting and drying leads to greater abundance of isolated pores during the drying than during imbibition (wetting) (Kiuru et al., 2022a).~~

Despite ~~these progresses~~ the progress in pore network ~~modelling~~modeling, experiments that demonstrate how peat pore networks regulate production of CO_2 and CH_4 ~~,~~ remain missing. One significant reason for this knowledge gap is the lack experimental approaches to localize biochemical reactions within intact peat cores. Most studies so far where conducted in mineral soils to identify anoxic microenvironments that allow for the oxygen-sensitive denitrification process to occur within a larger matrix of aerated soil (e.g. Kravchenko et al., 2017; Schlüter et al., 2018; Sihi et al., 2020). Most such studies focus on identifying correlations between pore network parameters, e.g. the distance of particulate organic matter to air-filled pores and macroscopically observed measures like N_2O emissions (Kravchenko et al., 2017; Rohe et al., 2021; Du et al., 2023; Ortega-Ramírez et al.). What remains missing is an approach to directly observe the biogeochemical reactions at a given locations within the soil pore network. Some progress has been provided by measurements with O_2 and N_2O microsensors (Rohe et al., 2021; Kim et al., 2021) and zymographic imaging (Kim et al., 2021, 2022). While such work has been conducted to identify N_2O producing microsites in agricultural soil, comparable work on CH_4 production in organic soils remains missing.

Here, we ~~aim to demonstrate~~ present an approach to study the microscale heterogeneity of both pore networks and biogeo-chemical processes within peat cores. To achieve this, we injected an isotopically labelled substrate ($^{13}C_2$-labelled sodium acetate, $^{13}CH_3COONa$) and followed the emissions of $^{13}CH_4$ and $^{13}CO_2$ from these cores during heterotrophic respiration (Reaction 1) and acetoclastic methanogenesis (Reaction 2). Note the position-specific conversion of C_2-carbon to methane in R2.

$$^{13}CH_3COOH + 2O_2 \rightarrow ^{13}CO_2 + CO_2 + 2H_2O \tag{R1}$$

$$^{13}CH_3COOH \rightarrow ^{13}CH_4 + CO_2 \tag{R2}$$

We compared the effect of injections at different depths and compared wetting and drying peat cores at the same water poten-tial on the conversion rate of the injected label into CO_2 and CH_4 as well as the time lag between the injection and the emission of these gases from the top of the peat core. After the manipulation experiment, we conducted microtomographic imaging and analysed the pore space above the injection depth. We hypothesize that greater air-filled porosity would be associated with a higher conversion of the methyl group of acetate to CO_2, less conversion to CH_4, and a more rapid onset of emissions.

2 Methods

2.1 Site description and peat sampling

Peat samples were collected from a forest (60°38′N, 23°57′E, Lettosuo, Tammela) in Southern Finland in December 2021. The site was drained in 1969 with parallel ditches in 40 m spacing. The mean annual temperature and precipitation at Lettosuo are 5.2 °C and 621 mm (Jokinen et al., 2021). The peat type iss Carex peat. The site was originally a mesotrophic fen classified as a herb-rich tall-sedge birch–pine fen (Laine and Vasander, 1996). The forest stand is dominated by Scots pine (*Pinus sylvestris*

L.) and downy birch (*Betula pubescens* Ehrh.) with an undergrowth composed of Norway spruce (*Picea abies* Karst.). The dominant height of the stand was 20 m and volume of the growing stock was 230 ~~m3 ha-1~~ $m^3 ha^{-1}$. Ground vegetation consists of dwarf shrubs (coverage 4 %) including *Vaccinium myrtillus* L. and *V. vitis-idaea* L., as well as herbs (coverage 10.6 %). A detailed site description is available in Kiuru et al. (2022a).

85   Peat core samples were collected from seven replicate pits that were located at least 30 m apart from each other. The cores were collected by removing the top 15 cm of soil, including a thin ice wedge that had formed in this layer. At each pit, two parallel samples were extracted into cylindrical cores (10.0 cm height, 10.0 cm diameter) from the depth of 15-25 cm.

2.2   Sample storage and water potential setup

Samples were wrapped in shrink-wrap foil and stored at +4 °C until the pretreatment, where all samples were water saturated
90   and placed on two sand beds that were hydraulically connected to hanging water columns (Eijkelkamp sand bed). One parallel sample from each pit was retained close to saturation (5 cm water column below the mid-point of the sample corresponding to a water potential of -5 hPa) while the other parallel sample was moderately drained (35 cm water column, i.e., -35 hPa). All samples were then set to a water potential of -20 hPa; consequently, one parallel sample of each pair reached the final water potential during drying and the other parallel sample during wetting.

95   ## 2.3   Measurement setup

For measurements, the peat samples were equipped with ca 7 cm high collars made from 5 mm thick neoprene rubber sheets that were outfitted with two ports for polytetrafluroethylene (PTFE) tubing. The bottom of each core and the top of each collar were sealed with shrink-wrap foil secured with rubber rings. One of the tube ports was connected to a 16-port selector valve (VICI model EMT-STF16MWE), and further to a Picarro G2201-i ($^{13}CO_2$/$^{13}CH_4$/H_2O) as well as a parallel pump for
100   increasing the flow rate through the measurement system (Fig. 1). The other tube port was equipped with a 1 m long tube open to the atmosphere. The total flow rate of the system was set to 500 mL min^{-1} by regulating the air flow to the auxiliary pump using a needle valve. In addition to the 14 peat samples, two empty chambers were included in the system as blank controls.

The measurement system was set up to pull air sequentially from each chamber for 10-minute periods. Each chamber was analysed once every 160 minutes, with a 150-minute break between the measurements, during which CO_2 and CH_4 were
105   allowed to accumulate in the chamber headspace. The time period between the two consecutive air pulling events in a sample is called hereon as a "closure". During the measurement event, the analyser initially measures the concentration and isotope values of CO_2 and CH_4 accumulated in the headspace since the previous measurement event of the chamber, followed by increasing dilution of the headspace with ambient air (Fig 2). After ca. 2-3 minutes, a dynamic equilibrium is reached where the headspace CO_2 and CH_4 concentrations equal the concentration in ambient air plus the current chamber emissions. The
110   closure times of the two empty chambers were slightly different (500 and 700 seconds) for easier identification of the chambers in the raw data.
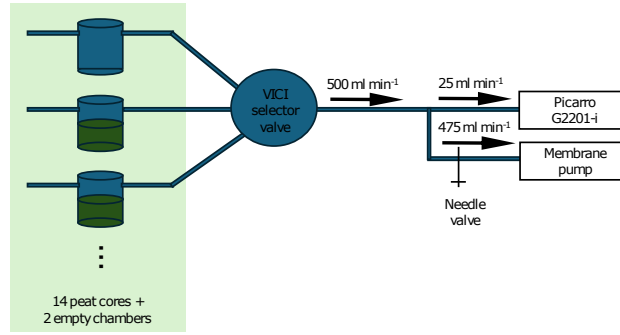
Figure 1. Depictions of the measurement setup. Ambient air was pulled through a headspace chamber to a Picarro G2201-i cavity ring-down spectroscopic $^{13}CO_2$/$^{13}CH_4$ analyser. A parallel line to additional membrane pump was used to increase the sample flow rate and regulate it with a needle vale. The system was connected to 16 chambers (14 peat cores and two empty chambers) using a VICI 16-port selector valve. Headspace air from each chamber was analyzed for 10 minutes once every 160 minutes, and CO_2 and CH_4 emitted by the peat cores was allowed to accumulate in the chamber headspace for 150 minutes between measurements.

2.4 Labeling experiment

^{13}C-labeled substrate was injected three times into each peat sample with ~~7~~ seven days intervals between injections. We injected 1 ml of 10 mM $^{13}C_2$-sodium acetate solution (i.e., a total of 10 μmol label per sample) followed by 1 mL ultrapure water. The injections were applied using syringes and hypodermal needles at 2.0, 5.0, and 8.0 cm depth. We permutated the order in which these injections were applied (2-5-8, 5-8-2, or 8-2-5 cm) in a different order for each pair of parallel sample.

After each injection, the needles were closed using 3-way valves to prevent gas exchange through the needle and left in the peat core for the rest of the experiment. After dismantling the experiment, the needles were removed to avoid metal objects interfering with microtomographic imaging and wooden toothpicks were inserted into the vacated needle canals to mark the position of the injections in the μCT image. However, the positions of these could not be identified in the μCT images, preventing the identification of the exact injection location in pore networks.

2.5 Flux calculations

For each chamber closure, we calculated the amount CO_2 and CH_4 emitted during a closure from the measured gas concentration using Eq. 3 after subtracting a baseline concentration determined by linear interpolation between the two closest blank measurements (Figs 2a, 2c, 2e, 2g). The emission rates (in mol $\min^{-1}$) were then calculated by dividing the amount of accumulated gas (in mol) through the time between measurements (160 minutes; Eq. 1).

$$F = \frac{A \cdot f}{V_{mol} \cdot t_{cycle}} \tag{1}$$
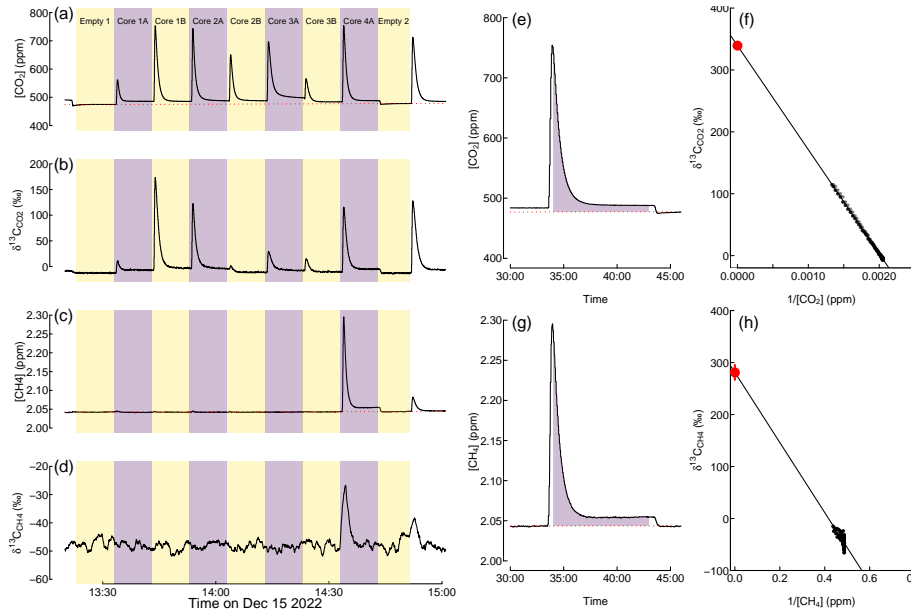
Figure 2. Example of raw data, including measured CO_2 and CH_4 concentrations (a, c), measured carbon isotope ratios ($\delta^{13}C$) in CO_2 and ~~CH4~~ CH_4 (b, d), integrated area for calculating CO_2 and CH_4 emissions rates (e, g), and Keeling plots for estimating the $\delta^{13}C$ value of peat-emitted CO_2 and CH_4 (f, h). The dashed red line in (a), (c), (e), and (g) represents the concentration baseline, which was estimated by interpolation from empty-chamber measurements. In (f) and (h), black symbols represent measured data points, solid lines represent linear regressions, and read points and error bars indicate the $\delta^{13}C$ value of peat-emitted CO_2 and CH_4 (i.e., the intercept of the regression line) and its 2 standard error uncertainty.

Where, F is emission rate (mol CO_2/CH_4 min^{-1}), A is the integrated baseline-corrected gas concentration from the maximum mixing ratio to 30 seconds before the end of the closure (mol CO_2/CH_4 mol^{-1} min), f is the gas flow rate (0.5 L min^{-1}),

130   ~~V_mol~~ V_{mol} is the molar volume of an ideal gas (24.055 L mol^{-1} at 20C and 101.325 hPa), and ~~t_cycle~~ t_{cycle} is the length of a measurement cycle (160 min).

We further calculated the ~~fraction of peat-derived and~~ f_i at each measurement time point i ~~according to eq. ?? (in the case of net emissions) or eq. ?? (in the case of net uptake), where c_i stands for the concetration at time point i, c_{bg} for the concentration in ambient air derived from empty chamber measurements, and c_min and c_max for the lowest and highest concentration during~~

135   ~~the measurement period.~~

$$f_i = \frac{c_i - c_{bg}}{c_{max}}$$

$$f_i = \frac{c_{bg} - c_i}{c_{min}}$$

Further, we then calculated the ~~Further, we then calculated the~~ carbon isotope values (δ^{13}C) values of CO_2 and CH_4 emitted during each ~~closures by mass balance as the~~ closure by the Keeling plot method, i.e., as the intercept of the linear regression between the measured δ^{13}C values and ~~1 − f (Figs 2f, 2h)~~ the inverse concentration (Figs 2f, 2h). We converted the δ^{13}C values to atom percent excess (APE) according to Eq. 2, where $\delta^{13}C_{sam}$ is the measured δ^{13}C value, $\delta^{13}C_{cont}$ is the δ^{13}C value of an unlabelled sample, assumed -28 ‰ for CO_2 and -70‰ for ~~, and R_ref~~ CH_4, and R_{ref} is the absolute ^{13}C/(^{12}C+^{13}C) ratio of the δ^{13}C reference material (VPDB; 0.01111233).

$$APE = \frac{\delta^{13}C_{sam} - \delta^{13}C_{cont}}{1000} \cdot R_{ref} \cdot 100 \tag{2}$$

The rate of label-derived CO_2 and CH_4 (F_L, mol min^{-1}) emissions were calculated based on the total emission rate F and the APE measured during each closure (Eq. 3).

$$F_L = F \cdot APE/100 \tag{3}$$

Eqs. 2 and 3 were also applied to quantify emissions of label-derived $^{13}CH_4$ from peat cores that showed net uptake of (unlabelled) CH_4. In that case both F and APE are negative, resulting in a positive F_L.

To correct for carry-over from one injection to the next (e.g. emissions of $^{13}CO_2$ and $^{13}CH_4$ derived from the first injection after the second injection) we fitted an exponential decay function to the $^{13}CO_2$ and $^{13}CH_4$ emissions rates over the four days prior to the next injection. This curve was then extrapolated to the measurement period after the subsequent injections and subtracted from the observed emissions.

To analyse the patterns of CO_2 and CH_4 emissions and compare experiments with slightly different runtimes, we calculated five measures for each injection. First, we calculated the average total (labeled + unlabeled) CO_2 and CH_4 emissions over the first 41 measurement cycles (109.3 hours) after injection. This measure serves primarily as a control for the impact of the incubation conditions and label injection on the overall functioning of the peat cores: any large change in total emissions after injections would indicate an alteration of microbial processes in the peat cores. Next, we calculated the fraction of the applied label emitted as CO_2 or CH_4 over the same time as an indicator of the local processes at the injection site. Finally, to characterize the combined effect of the delayed start of label conversion to CO_2, we determined the time from each label injection until half of the $^{13}CO_2$ emissions after the same injection had occurred ($t_{1/2}$).

2.6   Three-dimensional μCT imaging and image processing

After the labeling experiment, the peat samples were covered with shrink-wrap foil and stored in +4 °C until μCT imaging with a GE Phoenix Nanotom system (Waygate technologies). The flat panel detector was used in 4x4 bining mode, resulting in an effective pixel size of 100 μm at the sample. Two images were merged together at each projection angle by moving the detector sideways, in order to have large enough field of view to cover the whole sample laterally (merged projection image width 1104 x 100 μm). An exposure time of 1 second was used for each of the images. A CT scan was performed with 1200 projections

over a 360 degree rotation to obtain the data set. The X-ray generator voltage was 80 kV, and the current 120 μA. A 0.1 mm thick Cu sheet placed in front of the source was used as a beam filter. Three such CT scans were performed for each sample by moving the sample vertically to cover the whole height of the sample. The CT scans for each sample were then stitched into one stack of slices for further analysis. The scanning for each sample took 3 hours. The 16-bit 3D grayscale images obtained in the μCT reconstruction had size of 1268 by 1120 by 1120 voxels (cubic 3D image element) at 100 μm resolutions.

In the image preprocessing stage, the 3D grayscale images were converted to 3D binary images that separated void (air) voxels from voxels representing solid space and water using the Python image processing packages scikit-image ~~(Van Der Walt et al., 2014)~~ Van Der Walt et al. (2014) and SciPy ndimage (Virtanen et al., 2020) and the image analysis toolkit PoreSpy (Gostick et al., 2019). First, the 3D grayscale images were straightened and cropped to a size of 1000 by 900 by 900 voxels according to the inner dimensions of the cylindrical tubes. A cylindrical peat volume with a height of 1000 voxels and a diameter of 900 voxels was further selected using PoreSpy. Before the noise filtering and binary segmentation stages, the images were linearly mapped to an 8-bit representation. The mapping interval extended from 0.5 % to 99.5 % of the cumulative image gray-level intensity distribution so that the long tails of the intensity distribution formed by noise or occasional small mineral grains were removed. The 8-bit images were then noise-filtered using a 3D median filter with a 2-voxel radius. Finally, the images were segmented into void and solid volumes with the global Otsu thresholding algorithm (Otsu, 1979). Isolated solid regions were removed from the resulting binary images using a method for the determination of disconnected voxel space in PoreSpy.

2.7 Image analysis

Because the samples had shrunk slightly and their top and bottom surfaces were rough and uneven, the sample images were also cropped in the vertical direction so that the final image domain did not contain any external void space. The ~~height of the final cylindrical domain with~~ final cylindrical domains had a diameter of 90 mm ~~varied from~~ and a height of 75 ~~mm~~ to 95 mm. The air-filled porosity of each image domain was calculated as the ratio of the number of void voxels to the number of total voxels in the domain. The vertical air-filled porosity distribution was obtained by determining the void-voxel ratio for each horizontal voxel layer. For the determination of the radial air-filled porosity distribution, the domain was divided into 45 hollow cylinders with equal diameter increments. Because the samples had shrunk in the vertical direction, some void space had been generated between the peat matrix and the tube walls. To only include the internal void space of the samples, the vertical porosity distribution was calculated for a cylindrical domain with a diameter of 80 mm.

2.8 Pore networks

Pore networks were extracted from the final cylindrical domains of the binary images using a marker-based watershed segmentation method (Gostick, 2017). The segmentation algorithm divides the void space into individual pore regions and determines the connections between the pores and the locations of the two-dimensional interfaces between neighboring pores called pore throats. Because the feature resolution of a μCT-derived image is generally approximately twice the image voxel size (Stock, 2008; Elkhoury et al., 2019), the size of the smallest distinguishable feature in the images was 200 μm.

The pore system generated by the extraction algorithm was divided into clusters of interconnected pores and a group of single isolated pores using the open-source pore network modeling package OpenPNM (Gostick et al., 2016). The largest of these clusters, which was assumed to be the only cluster that extends through the network domain in the axial direction and which was therefore the relevant space regarding gas transport through the domain, was defined as the pore network. The pore volume was determined by counting the number of voxels in an individual pore region. Network porosity was defined as the ratio of the sum of the volumes of the pores in the network to the total volume of the domain. Further network metrics were calculated following Kiuru et al. (2022a). Briefly, coordination number is defined as the average number of connections of each pore to other pores. Clustering coefficient as the probability that two pores connected to a given pore are also connected to each other. Closeness centrality is the reciprocal of the average shortest path length from one pore to each other pore in the network. Geometrical tortuosity and betweenness centrality represent ~~transport~~ properties of the pore network ~~a~~ that affect gas transport in certain direction (between top and bottom of the peat core) and as a whole.

2.9 Statistical analysis

~~We tested for treatment effects on parameters discribing~~ To identify effects of soil moisture treatments on air-filled porosity and pore network metrics (coordination number, clustering coefficient, geometric tortuosilty, closeness centrality, and betweenness centrality), we applied a mixed effects model that used treatment as a fixed effect and soil pit as a random effect (n=14). Further, to quantify the fraction of variance explained by pit-to-pit variability, we first applied one-way analyses of variance (ANOVA) with moisture treatment as the sole predictor to remove potential treatment effects. We then the calculated the fraction of variance in the residuals explained by soil pit in second ANOVA. As our focus in this analysis was to compare the explained variance across different dependent variables, we present the fraction of variance explained regardless of statistical singificance.

To test for potential disturbances due to repeated labelling or prolonged incubation, we tested for changes in total (labeled + unlabeled) CO_2 emissions after each injection (n=42) by applying a mixed effects model where injection depth, injection round, and moisture treatment were set as fixed effects and while soil pit and core (within soil pit) were chosen as random effect.

To test the effects of injection depth on other parameters derived from label injection experiments (n=42), we applied a mixed effects model that used treatment and injection depth as fixed effects while soil pit and core (within soil pit) were used as random effect. Injection round was added to the model to control for potential changes over time during the incubation. As the limited replication did not allow the statistical analysis of potential interaction effects, we split the dataset into the drying and wetting subsets (n=21) and repeated the analysis with injection depth as a fixed effect and core as a random effect.

To test for treatment effects on parameters describing CO_2 and CH_4 emissions by applying mixed effect models. We applied *injection depth*, *injection round*, and *moisture treatment* as fixed effects and *soil pit* as a random effect. ~~For fixed effeest~~ Not interaction effects were considered in this model. For fixed effects that significantly affected the dependent variable, we conducted estimated marginal means to identify significant differences between variable levels. ~~In addition to these models~~

Finally, to investigate whether air filled porosity derived from the μCT images can explain the heterogeneity of label-derived

235   CO_2 emissions between peat cores and injections, we tested ~~for linear~~ whether the average air filled porosity above injection depth was correlated to the fractions of the label emitted as CO_2 or $t_{1/2}$. This analysis was performed separately for each injection depth. We also tested for correlations between pore network ~~measures and~~ metrics, label-derived CO_2~~flux parameters,~~ and $t_{1/2}$, as well as for correlations between these predictors. All statistical analysis was ~~conducted~~ performed in the statistical programming environment R version 4.2.1 (R Development Core Team, 2015) using the *lme4*, *lmerTest*, and *emmeans*

240   packages.

3   Results~~and discussion~~

3.1   Microtomography and pore architecture

~~The mean air-filled porosity in the 14 peat samples ranged 0.20 to 6.75% (average: 2.56%, standard deviation 2.02 %).~~ Microtomographic imaging revealed high heterogeneity both within and between the peat cores. Four examples of vertical cross

245   sections through the cores are shown in Figs. 3 and S1. Visual inspection showed large, mainly horizontally-oriented macropore systems in a dense matrix (Figs 3a,3c,3d), and vertically connected pore networks (Fig 3b) reflecting a looser peat structure. We found a large degree of vertical heterogeneity in air-filled pore-volume, originating from layered, horizontally oriented macropores (Fig. 3e) and air-filled cavities in the peat samples. In contrast, all peat cores show the same radial porosity trend from the center to the edge (Fig 3f). This indicated the absence of distinct vertical pore structure, which would be visible

250   distinct features in these plots. All samples showed a similar increase of air-filled porosity towards the edge of the sample, an artifact of shrinkage caused by drying.

~~The visible structure of the peat reflects the original plant residues that formed the peat at the site as well as the changes during over time and the effects of site drainage. In forested peatlands the peat typically contains woody plant fragments and Carex residues, as is the case at Lettosuo. Woody fragments in peat increase spatial heterogeneity with large macropores compared~~

255   ~~to the more fine-pored and homogeneous sphagnum-derived peat (McCarter et al., 2020). The presence of dwarf shrubs likely also introduced looser peat structure and larger macropores. Site drainage enhances peat decomposition, which leads to a loss in macropore space and increases peat bulk density, particularly in the top layer of the peat (Minkkinen and Laine, 1998). Concurrent with the enhanced decomposition and compaction, a raw-humus layer forms on top of the peat. The raw humus layer is mainly formed of litter originating from upland vegetation and might have influenced the underlying layer from which~~

260   ~~the samples in this study were collected, e.g.by forming a horizontally layered peat structure (Lauren, 1999).~~

~~Scanning whole peat cores required us to limit the measurement resolution to 200 μm. We thus captured only the largest of macropores. However, this resolution was sufficient to map~~ Metrics describing network traits are shown in Fig. 4. For most network metrics, the high heterogeneity of pore networks across peat cores prevented us from identifying statistically significant differences between wetting and drying treatments. We have, however, identified several non-significant trends that

265   may be relevant for interpreting the results of our label injection experiments. The mean air-filled ~~pores in our samples, which were set to a water potential of −20 hPa. This corresponds to an equivalent pore size diameter of 150 . We were unable to identify~~
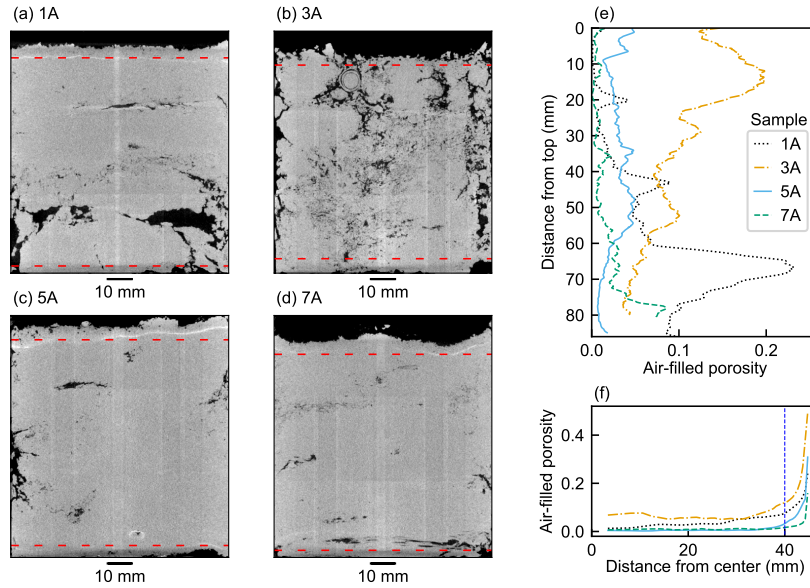
Figure 3. Axial cross sections of noise-filtered 3D μCT images of peat samples (a) 1A, (b) 3A, (c) 5A, and (d) 7A. Air-filled pore space is displayed in black and peat in white. Further, vertical (e) and radial (f) profiles of the air-filled porosity of the samples. Red dashed lines in the images show the boundaries of the final network domain.

the injection positions marked by wooden toothpicks used to mark them. We can therefore only compare GHG emissions to properties at the scale of the scanned peat cores, but not the local environment at the location of the injection porosity in the 14 peat samples ranged 0.20 to 6.75% (average: 2.56%, standard deviation (SD) 2.02 %). Overall, air-filled porosity did not
270 differ between wetting (2.62±2.10% (mean±SD) and drying soils (2.30±2.10%) (Fig 4a). While we found no difference in the air-filled pore volume of the whole core between treatments, we detected a (non-significant) trend towards a larger number of individual pores in wetting than in drying treatments, i.e., the wetting treatment lead to a smaller average pores volume (Fig 4a). We further observed (non-significant) trends towards a larger number of pores and a greater pore volume not connected to the main network in wetting treatments (not shown). Moreover, the wetting treatment had significantly lower coordination
275 numbers and clustering coefficients compared to drying treatments (Fig 4b-c). In contrast, we find no significant difference between treatments in geometric tortuosity, closeness centrality, and betweenness centrality (Fig 4d-f).

This simlarity in average porosity masked differences between the treatments that became apparent in network metrics and when air-filled porosity was analysed by depth layer. Air filled porosity did not differ in shallow layers (0-2 and 2-5cm), although we did observe a non-significant trend towards higher air-filled porosity in drying treatments (Fig 4a). In contrast, we
280 found significantly higher air-filled porosity in wetting than in drying treatments in deeper layers (5-8 and 8-10 cm).
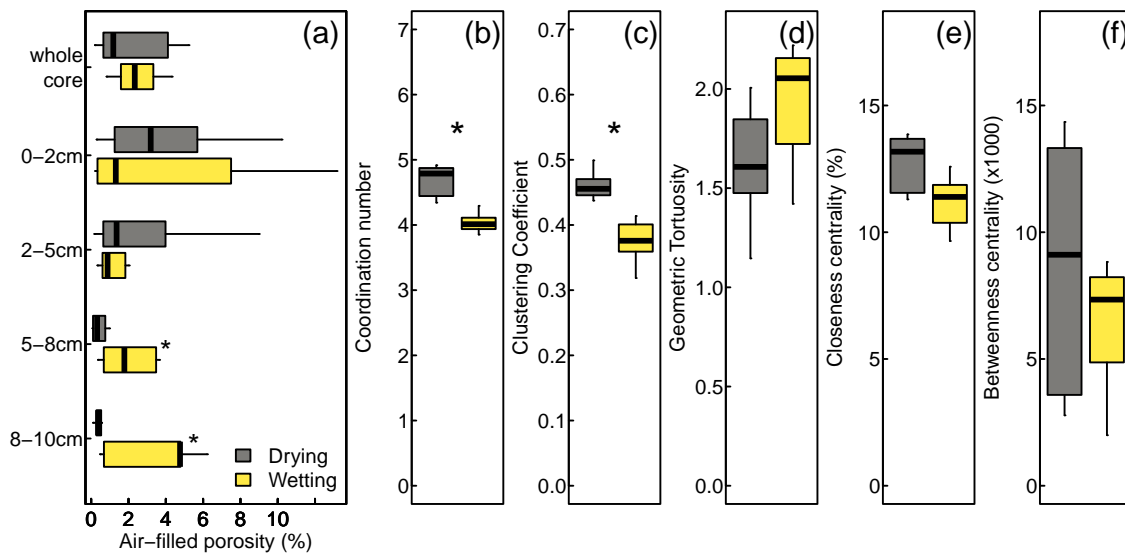
Figure 4. ~~Axial cross sections of noise-filtered 3D μCT images of peat samples~~ Moisture treatment effects on air-filled porosity (a) ~~1A, (b)~~ ~~3A, (c) 5A,~~ and pore network metrics (d) ~~7A as well as vertical (e~~b-f)~~and radial~~. Asterisks indicate significant differences between treatments (f*, $0.01 < p < 0.05$)~~profiles of the air-filled porosity of the samples. Red dashed lines in the images show the boundaries of the final network domain~~Betweenness centrality values have been multiplied by 1000 for easier readability.

3.2 CO_2 and CO_4 emissions from peat core

3.2.1 Background emissions of CO_2 and CH_4

All peat cores emitted CO_2 at a mean rate of 1.6 ± 0.6 ~~(1 SD among core)~~ µmol h^{-1} (1 SD among cores; range: 0.4 to 2.7 µmol ~~h~~h^{-1}). These total emissions were not affected by the injections, as was indicated by the lack of differences of the background respiration after the injections at different depths (Fig 5a). We did, however, observe ~~a trend towards~~ ca. 20% higher CO_2 emissions after the third round of injections (Fig 5b ~~) that approach significance (p = 0.076). This indicates the potential for~~ indicating a minor increase in peat respiration rates towards the end of the experiment. We observed no differences between the drying and wetting treatments (Fig 5c).

Three of the 14 peat cores acted as methane emitters with emissions rates up to 1.67 nmol h^{-1}, whereas the remaining 11 peat cores acted as small ~~CH4~~ CH_4 sinks with sink strength up to 0.05 nmol ~~h~~h^{-1}. On average, the peat cores were net emitters with ~~a~~ an arithmetic mean flux of 0.32 ± 0.95 nmol ~~CH4 h~~CH_4 h^{-1}. All methane-emitting cores had low air-filled porosities (<1%), although not all cores with low air-filled porosity emitted methane. We observed no significant changes in the background CH_4 emissions over the course of the experiment and no difference in emissions after the injections at different depths (Fig 5d-5e). A trend towards higher emissions in drying compared to wetting treatments (Fig 5f) was not significant (p=~~0.086).~~

~~The absence of methane emissions from most peat samples was consistent with the field environment where they were collected: a drained peatland that currently acts as a net sink of methane (Korkiakoski et al., 2020). The water potential in our experiment (-20 hPa) was comparable to the location of the water table (-40 to -30 cm)relative to the sampling depths. Our results thus indicate the presence of individual methane emitting locations in a larger methane consuming stand.~~

~~The independence of background and emissions of injection depths indicates that the label (acetate) injections did not affect the overall biogeochemistry of the peat cores (Fig. 5a, 5d). However, it is possible that the peat cores were affected by higher temperatures, which may have increased the respiration rates towards the end of the experiment. Nevertheless, the size of this disturbance was limited and acceptable in an experiment that was not designed to exactly replicate field conditions.~~

~~The trend towards higher methane emissions in the wetting compared to the trying treatment is interesting, as it indicates higher methane emissions in peat cores that have been exposed to more oxic conditions prior to the experiment. This may have been caused by the release of more labile substrates during aerobic episodes which can then be utilized by methanogens during the following aerobic period~~~~0.96).~~

3.3 Label-derived ~~2~~ CO_2 emissions

We followed the release of the label-derived $^{13}CO_2$ over 43-68 measurement cycles, that is, 114-181 hours. ~~In these emissions, we~~ We observed a high heterogeneity in these emissions between the peat cores and in the response to individual injections (Fig. 6). Overall, we observed the highest rates of $^{13}CO_2$ release over the first 24 hours after label injection (Figs. 6a-6c). However, only some of the injections led to a strong, early $^{13}CO_2$ release. Other injections showed a longer response time lag, reaching maximum $^{13}CO_2$ emission rates 24-72 hours after the label injection. Although this type of response typically showed lower maximum emission rates (Figs. 6a-6c), it often reached a higher cumulative emission throughout the experiment (Figs 6d-6f).

To compare $^{13}CO_2$ emissions across experiments that had different runtimes, we integrated the observed emissions over the first 41 measurement cycles (109.3 hours). Over this period, we found emissions ranging from 0.01 to 1.22 μmol $^{13}CO_2$ or 0.11 to 12.2% of the injected label. The average fraction of the label emitted as CO_2 decreased with injection depth, from 7.2% at 2 cm depth to 1.9% at 8 cm depth (F=12.2, p <0.001; Fig 7a). This depth effect was found in both wetting and drying cores. The emitted $^{13}CO_2$ did not differ between the injection rounds or soil moisture treatments (Figs 7b, 7c).

To characterize the combined effect of the delayed onset of the label conversion to CO_2 and the diffusion time, we determined the time from each label injection ~~til~~ until half of the $^{13}CO_2$ emissions after the same injection had occurred ($t_{1/2}$). This level was reached after 3 to 28 hours. Again, we found a significant difference between injections at different depths, with $^{13}CO_2$ emissions showing a greater average time lag at greater depths (10.5 hours at 2 cm depths vs. 17.1 hours at 8 cm depths). A more detailed analysis, however, showed that this was only true among wetting soil cores, while injection depth had no effect on $t_{1/2}$ in drying cores. Further, injection round or soil moisture treatment had no significant effect on $t_{1/2}$.

~~The slower or time-delayed emission of after injections at greater depth could have been caused by several factors. The water potential differs within the peat cores according to hydrostatic equilibrium, with wetter conditions at the deeper layers. This results in a smaller air-filled porosity, and less connected pore space. Microorganisms in deeper layers are therefore~~
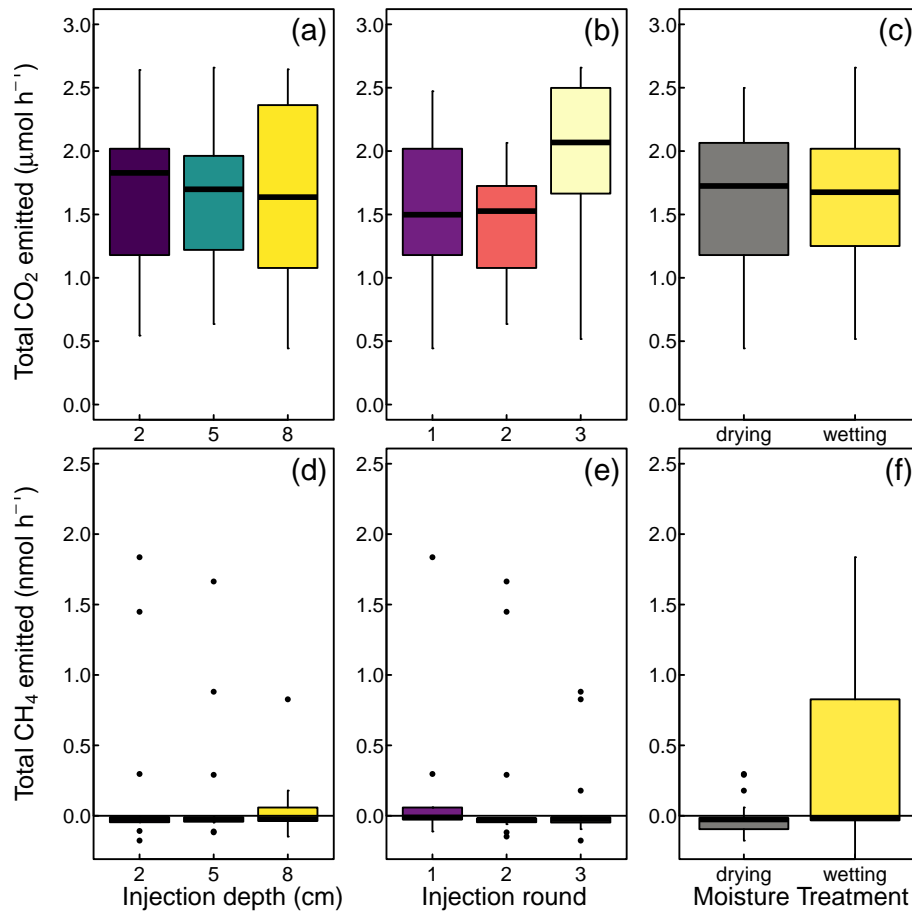
Figure 5. Total carbon dioxide (CO_2) and methane (CH_4) emissions from peat cores, that is, the sum of label-derived and non-label-derived emissions. Positive numbers indicate net release of gases to the atmosphere, negative numbers net uptake by the peat cores. Letters in panel (b) indicate significant differences between the injection rounds. No significant differences were found in any other case.

330 ~~exposed to a more oxygen depleted environments. Deeper layers are also characterized by a smaller interface area between the air- and water-filled pores than the shallow layers, which limits the space where the fast heterotrophic respiration is feasible. Furthermore, these layers are more distant from the surface, and pore networks likely show greater tortuosity, which leads to a greater resistance to diffusion of oxygen from the surface to these layers, and vice versa, diffusion of CO2 to the surface.~~

~~The two measures (~~After this initial analysis, we split the dataset to separately analyse depth and injection round effects

335 in wetting and drying cores. This analysis resulted in contrasting results for the different measures. For cumulative $^{13}CO_2$ ~~produced and $t_{1/2}$) showed great variance that was only partially explained by the main variables in our study (injection depth, injection round, moisture treatment, soil pit), with 31% residual variance in the case of label-derived CO2 and 41% residual variance for $t_{1/2}$ **(Fig S2)**. This large unexplained variance likely resulted from difference among individual soil cores and spatial variability within the cores, and therefore likely represents heterogeneity in peat structure (i.e., pore networks). Injection~~
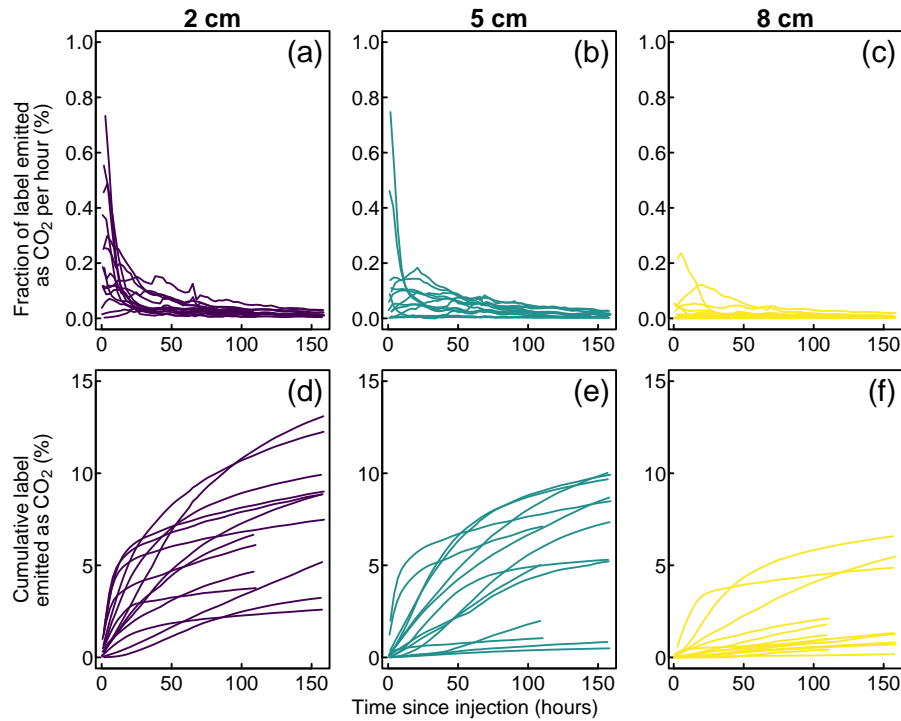
Figure 6. Instantaneous (a-c) and cumulative (d-f) emissions of label-derived CO_2 grouped by injection depth.

~~depth explained 38% of the total emissions of label-derived~~ emissions, both treatments show the same response found in the overall data set, that is, less of the injected label was emitted as CO_2 ~~and 15% of~~ after deeper injections (Fig. 8a-b). In contrast, we find distinct responses of the timing of $^{13}CO_2$ release ($t_{1/2}$. ~~Pit-to-pit variation was an important predictor for~~) in wetting and drying treatments, with injection depth having little effect on $t_{1/2}$ ~~(43% variance) , but not for the amount of (produced. All other independent variables explained less then 10% of the variability~~in wetting treatments (Fig. 8c) but greater depth leasing to a slower release in drying treatments (Fig. 8d).

3.4 Label-derived CH_4 emissions

The label-derived CH_4 emissions ~~of were highly heterogeneous~~ showed highly variable responses to the individual label injections (Figs 9a-9c). Quantitatively, however, the conversion of the injected label to ~~CH4~~ CH_4 was very limited, with less than 0.01% of the injected label emitted as methane. We detected $^{13}CH_4$ emissions in both peat cores that showed background (non-labelled) CH_4 emission and peat cores that showed no such background emission, but $^{13}CH_4$ emissions increased with higher background emissions (R >0.73, p <0.003, tested separately for each injection depth).

Not all label injections into methane emitting cores resulted in $^{13}CH_4$ emissions. Rather, we found differences between injections into the same peat core, further highlighting within-core heterogeneity. Injections into one of the peat cores (sample
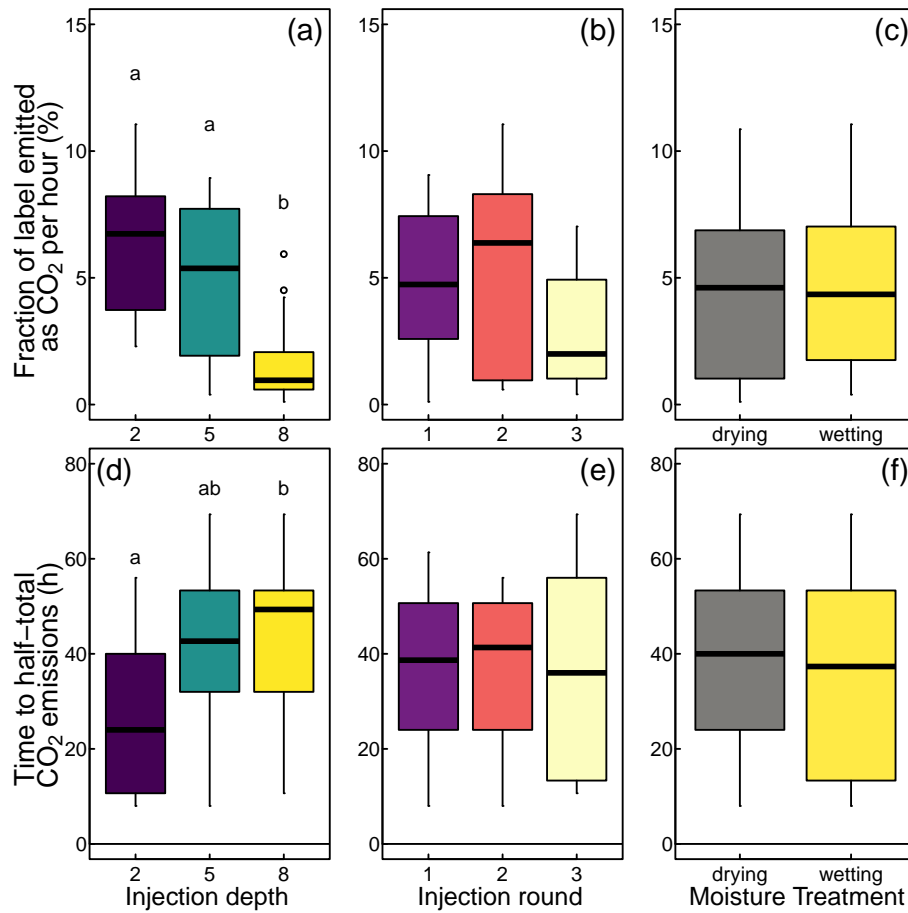
Figure 7. Effects of injection depths, injection round, and moisture treatment on the fraction of the label emitted as CO_2 and delay to half-total emissions. Letters indicate significant differences between groups.

7A), for examples, resulted in situations (i) large $^{13}CH_4$ with little $^{13}CO_2$, (2) emissions of both $^{13}CH_4$ and $^{13}CO_2$, and (3)

355 only $^{13}CO_2$ (Fig. 9d). This response was not a simple function of depth – highest ~~13CH4~~ $^{13}CH_4$ emissions were found after injection at intermediate depths, while highest CO_2 emissions were found after injection into deepest layer.

~~Our results thus show~~

4 Discussion

4.1 μCT images represent typical peat from peatlands drained for forestry and are suitable for pore network

360 modeling at the low water tensions that prevail at such sites
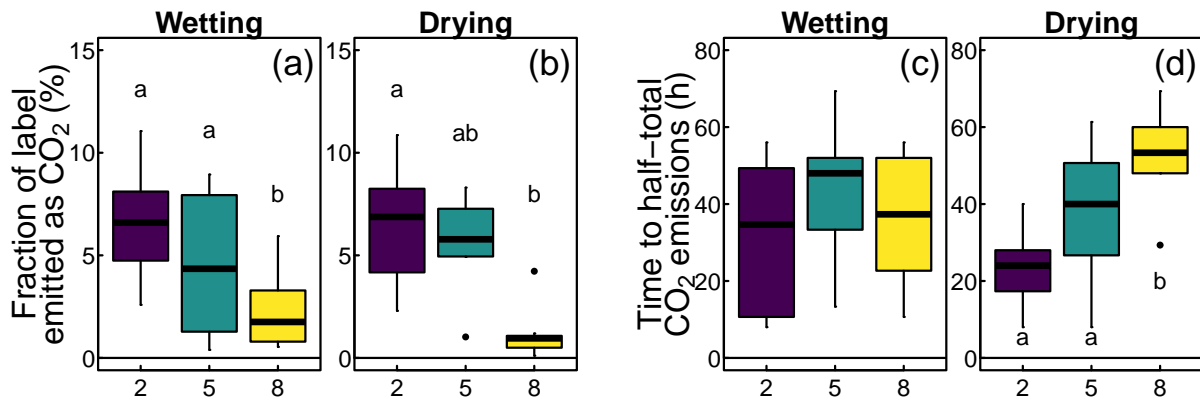
Figure 8. ~~Effects of injection depths, injection round,~~ Depth effect on amount and ~~moisture treatment Fraction~~ timing of ~~the label emitted as CO2 and delay to half-total~~ label-derived CO_2 emissions.
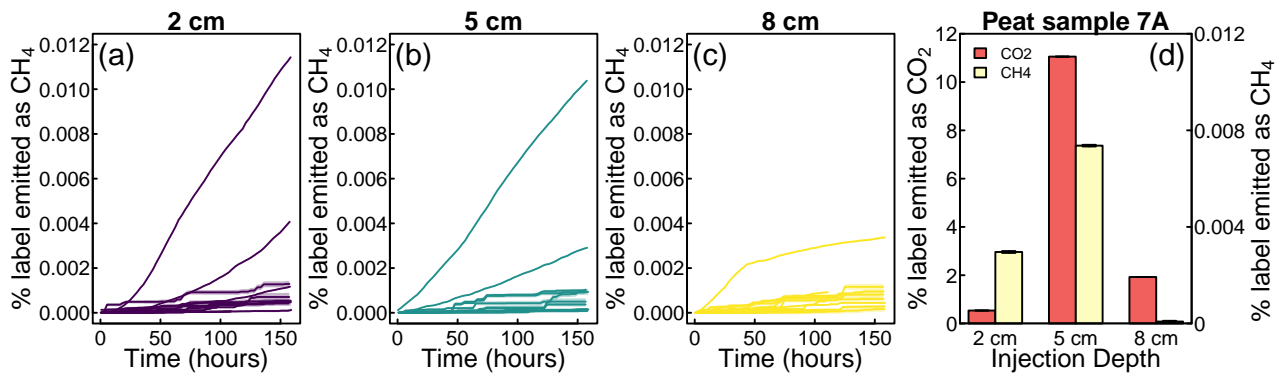
Figure 9. Cumulative emissions of label-derived CH_4 grouped by injection depth (a-c). Further, a comparison between label-derived CO_2 and CH_4 emissions after injections at different depth into an example peat core (d).

The structures revealed by μCT imaging of the peat reflect the original plant residues that formed the peat at the site, as well as the changes over time and the effects of site drainage. In forested peatlands, the peat typically contains woody plant fragments and Carex residues, as is the case at Lettosuo. Woody fragments in peat increase spatial heterogeneity with large macropores compared to the more fine-pored and homogeneous Sphagnum-derived peat (McCarter et al., 2020). The presence

365 of dwarf shrub roots and rhizomes likely introduced looser peat structure and larger macropores. Site drainage, in contrast, enhances peat decomposition, which leads to increasing peat bulk density and a loss in macropore space, particularly in the top layer of the peat (Minkkinen and Laine, 1998). Concurrent with the enhanced decomposition, subsidence and compaction, a mor-humus layer forms on top of the peat (Hökkä et al., 2024). The mor humus layer is mainly formed of litter originating from upland vegetation and might have influenced the top part of the sample, e.g. by forming a horizontally layered pore

370 architecture, affecting gaseous diffusion (Ballard, 1970; Laurén and Mannerkoski, 2001).

Scanning whole peat cores with a 100 mm diameter and height required us to limit the measurement resolution to 200 μm. Although we captured only the largest of macropores, this enables us to study the architecture of the air-filled pore network that dominates the gas exchange in peat. At the water potential of our samples (–20 hPa), for example, only pores with an equivalent diameter larger than 150 μm are typically air-filled. Conversely, the large image domain allowed us to study the long-distance (centimeter scale) transport of gasses throughout the peat cores and properties of the pore network. Our resolution is therefore significantly lower than in other recent studies that focus on anoxic processes in unsaturated mineral soil (e.g. denitrification), where the relevant size is smaller and where researchers have to focus on a more detailed analysis of a smaller image domain. For example oxygen diffusion was estimated to reach e.g. 35 μm distance to the closest pore (Kravchenko et al., 2017).

4.2 Hysterectic behavior during drying and wetting led to distinct water distribution within peat cores and in pore networks with distinct network properties

Our experimental treatments were successful in so far as they allowed us to reach comparable air-filled porosity (indicating similar water content) from drying and wetting directions. Despite this similarity in average moisture content, these treatments led to differences in the water distribution within the cores and the structure of the air-filled pore networks. Drying treatments led to an accumulation of water in the top layers of the peat and in networks with higher coordination numbers and clustering coefficients, while wetting treatments led to an accumulation of water near the bottom of the core and in networks with lower coordination numbers and clustering coefficients.

These results demonstrate the hysteresis during drying and wetting has been studied theoretically (Mualem, 1974) and with models (Ball, 1981; Vidal-Beaudet and Charpentier, 2000), and experimentally macroscopic scale (e.g. Chen et al., 2024; Bratbak and Dun and with microtomographic imaging (Pires et al., 2020; Pan et al., 2024; Mady and Shein, 2020; Higo and Kido, 2023). Differences between wetting and drying treatments can be explained by the ink bottle effect (Mualem, 1974): water flow out of peat cores is limited by the smallest throat, while water flow into peat cores is limited by pore size. The representation of these effects in empirically measured pore networks, has been theoretically evaluated (Ball, 1981), but this has not been applied to actual μCT derived pore networks. The differences in pore network structure and within-core water distribution likely affect gas diffusion in the peat core in opposite directions. The higher coordination number and clustering coefficients in dry) indicate greater connectivity of the pore space in drying than in wetting treatments, which could lead to gas higher gas diffusivity in drying cores at a given air-filled porosity. Drying treatments, however, also led to the establishment of a layer with relatively high water content on the top of the peat cores, which may restrict gas exchange between the peat pore network and the atmosphere.We would therefore expect a better aeration of the most shallow peat layer (above the depth of most label injections) in wetting treatments, but better connectivity between top and deep peat layers in drying treatments.

It is worth noting that these effects are to some degree specific to our experimental setup, which simulated water movement due to changes in the water table, i.e., changes in the water potential applied at the bottom of the peat core, while peat cores were open to air at the surface. Our experiment is therefore not representative for wetting by rainfall, when water infiltrates from the top of the peat column.

Constant background emissions of CO_2 and CH_4 indicate little overall disturbance due to label injection. All samples emitted (non-labeled) CO_2 as is expected from soil samples. With the exception of moderate increases after the third injection round, we did not detect changes in the non-labelled CO_2 emissions during the experiment. This indicates that the label injections had only a local impact and did not alter the biogeochemistry elsewhere in the peat cores. The slight increase in CO_2 emissions after the third injection round indicates a minor stimulation of microbial activity after prolonged exposure to incubation conditions, i.e., higher temperature during the experiment (13-20 °C) than the storage temperature prior to the experiment (4 °C). Nevertheless, the magnitude (<20%) of this disturbance was limited and acceptable in an experiment that was not designed to exactly replicate field conditions.

The absence of methane emissions from most peat samples was consistent with the field environment where they were collected: a drained peatland that currently acts as a net sink of methane (Korkiakoski et al., 2020). The water potential in our experiment (-20 hPa) was comparable to the location of the water table (-40 to -30 cm) relative to the sampling depths (-15 to -25cm). Our results thus indicate the presence of individual methane emitting locations within a larger methane consuming stand. The trend towards higher methane emissions in the wetting compared to the drying treatment is interesting, as it indicates higher methane emissions in peat cores that have been exposed to more oxic conditions prior to the experiment. This may have been caused by the release of more labile substrates during aerobic episodes which can then be utilized by methanogens during the following wetting. Peat cores in the wetting treatments also exhibited more poorly connected pore networks, and higher pore numbers and pore volumes not connected to the main pore network. This makes the presence of anaerobic pockets more likely in wetting than in drying treatments, even though both treatments had comparable overall air-filled porosity (Kiuru et al., 2022a).

Label injections allow visualizing differences in biogeochemical transformations. A novel aspect of our work was our attempt to directly demonstrate the spatial heterogeneity of biogeochemical transformation rates by injecting a ^{13}C-labeled substrate at specific locations in the peat core and then following the release of $^{13}CO_2$ and $^{13}CH_4$ into the headspace. Our automated measurement setup with a CRDS online isotope analyser allowed for the simultaneous and continuous monitoring of these emissions in 14 replicate cores. With this experiment, we provide an approach to study the heterogeneity of biogeochemical transformation that can provide information that is complementary to other methods like zygometry (Kim et al., 2021, 2022), microsensors (Rohe et al., 2021; Kim et al., 2021), or the correlative analyses of pore network properties with macroscopic measures like greenhouse gas fluxes (Ortega-Ramírez et al., 2023; Rohe et al., 2021; Du et al., 2023). Our approach complements these methods by allowing for a direct quantification of local (potential) biogeochemical process rate, rather than the local chemical environment (e.g. the local redox conditions in microsensor measurements). Our method differs from zygometry in that it is relatively non-invasive and can be repeated within a given soil sample through multiple label injections at the same or different locations.

Our results show that the injection of 10 μmol of $^{13}C2$-labeled acetate was sufficient to produce a strong $^{13}CO_2$ signal in all peat cores without significantly altering the background CO_2 emissions, indicating little impact outside the immediate injection location. Noteworthy, we applied the label in a relatively large volume of water (1 mL), which limited the spatial resolution of our experiments to the centimeter scale. For better spatial resolution, future experiments should reduce this volume. This will,

however, require balancing the introduction of a sufficient label amount to produce detectable $^{13}CO_2$ fluxes whilst avoiding increasing the substrate concentration at the point of injection. The relatively low resolution means that our approach is likely of greater use for visualizing CO_2 and CH_4 production organic soils with heterogeneity at the millimeter to centimeter scale, compared to N_2O production in mineral soil where small-scale structures (tens of micrometers) are of great importance for local oxygen availability (Kravchenko et al., 2017).

We originally aimed at identifying the local environment at the injection locations in μCT images and pore networks, but we were unable to consistently identify these locations due to the poor visibility of our markers (wooden toothpicks) in μCT images. We can therefore only compare GHG emissions to properties at the scale of the scanned peat cores, as we were not able to study the local environment at the very location of each injection. Such characterization of local injection environments is a future direction of development for this method.

4.3 Differences in the amount and timing of label-derived CO_2 release between injection depths indicates differences in biogeochemical process rates rather than differences in gas transport

Our finding of systematic differences in the amount of label-derived CO_2 emissions after injections at different depths may have resulted from two processes. First, microorganisms might be more active in shallow layers than in deep layers, thus producing more $^{13}CO_2$ during the duration of the experiment. This represents the local biogeochemical heterogeneity we intended to measure. Second, the greater distance to the surface from deeper layers means that microorganisms could have produced the same amount of $^{13}CO_2$ after all injections, but when injections were conducted at greater depth less of it would have reach the headspace before the end of the experiment . This would be a confounding effect in our measurements. This confounding effect, however, was likely small in our experiments as gas diffusion is relatively fast at the range of air-filled porosity present in our study (1-5%) (e.g. Bartholomeus et al., 2008). Previous measurements in peat cores collected at the same site and depths and at comparable water potential (-30 to -10 hPa) found gas diffusivities between 2×10^{-3} and 1×10^{-2} cm^{-2}s^{-1} (Kiuru et al., 2022b) corresponding to diffusion lengths of between 8.8 and 19.6 cm over one measurement cycle (160 minutes), i.e., larger than our peat cores. It is therefore unlikely that the lower amount of label-derived CO_2 emitted after deeper injection was driven by limited diffusion out of the peat core. This is further supported by the time courses of CO_2 release from 8cm deep injections, which in many cases had their maxima within the first half of the experiment (Fig 6c). Further evidence is provided from the independence between the amount and timing of label-derived CO_2 emissions between moisture treatments. While both treatments show less label-derived emissions after injections at greater depth (Fig 8a-b), only peat cores from the drying treatment showed that these emissions occurred more slowly at greater depths (Fig 8c-d). If differences in the amount of label-derived CO_2 emissions were driven by delay due to the diffusion distance, we would expect a similar response of these two measures in the two treatments. Given this evidence, we are confident that the measured differences in the amount and timing of label-derived CO_2 emissions represents differences in microbial activities rather than differences in gas transport.

Our finding of different amounts of label-derived CO_2 emissions after injections at different depths therefore indicates vertical differences of (potential) microbial activity within the peat core, with greater activity in layers located closer to the

surface. Such a greater activity could be a result of higher oxygen availability in layers with better connection to the peat surface. The activity we measured should be considered potential as we likely significantly increased the local substrate concentrations

475 at the point of injection (injected concentration 240 mg C l^{-1}) and because the higher activities in shallow layers have been limited by local substrate depletion. Nevertheless, the difference is quite stark, with a ca. five-fold higher respiration activity at 8 cm than at two centimeters. These results thus suggest a high spatial heterogeneity in the (background) respiration in peat cores - most CO_2 is derived from the peat layer closest to the surface. This challenges the assumption made in most experiments with peat columns that microbial processes occur homogeneously throughout the peat column.

480 The different depth effects on the timing of $^{13}CO_2$ emissions from drying and wetting peat cores suggest that microorganisms respond more slowly to a sudden increase in (labeled) substrate availability. This was likely due to lower overall activity in drying treatments, which were characterized by particularly high water content in deep layers, suggesting that oxygen availability was relatively low in the deep layers. This is also supported by the (non-significant) trend towards higher (non-labeled) methane emissions in the wetting than the drying peat cores. This trend was interesting, as it indicates higher methane emissions

485 in peat cores that have been exposed to more oxic conditions prior to the experiment. This may have been caused by the release of more labile substrates during aerobic episodes which can then be utilized by methanogens during the following aerobic period.

4.4 Methanogenesis exhibits high spatial heterogeneity

Our finding of highly heterogeneous $^{13}CH_4$ emissions shows that methane production varied both at the scale of tens of

490 centimeters (replicate injections into the same core gave similar responses), and at the cm scale (contrasting results from injections into the same peat core). This highlights the great heterogeneity of peat at sub-site scales. It also indicates presence of methane-generating and non-methane-generating locations within peat cores, likely corresponding to the oxic and anoxic microsites within peat cores ~~(Fan et al., 2014).~~

(Fan et al., 2014). The tracing of label-derived CH_4 in our study remained associated with some important limitations. First,

495 we measured $^{13}CH_4$ emissions, which differ from $^{13}CH_4$ production. It is likely that the anaerobic pockets where $^{13}CH_4$ is formed are poorly connected to the surface, and that the formed $^{13}CH_4$ may not reach the sample headspace. Indeed, the most $^{13}CH_4$ emissions time series (Figs ~~9a-9c~~7a-7c) show continuous emissions over the whole ~~timecourse~~ duration of the experiment, unlike $^{13}CO_2$ emissions which ~~decreased over time 6~~often decreased after 24-48 hours (Fig. 6). This may indicate that acetoclastic methanogenesis occurs more slowly than heterotrophic respiration, consistent with the slower nature

500 of anaerobic metabolisms. It may also indicate that $^{13}CH_4$, once formed in anaerobic pockets with poor connectivity to the peat surface, reaches the sample surface ~~only slowly~~more slowly than CO_2. Another limitation is that we cannot exclude that $^{13}CH_4$ formed at the site of the label injection is oxidized by methanotrophs prior to reaching the peat surface.

~~Cumulative emissions of label-derived grouped by injection depth (a-c). Further, a comparison between label-derived and emissions after injections at different depth into an example peat core.~~

4.5 ~~Comparison between~~ Air-filled porosity ~~,~~ has a stronger impact on biogeochemical process rates compared to pore network ~~properties, and greenhouse gas emissions~~ metrics

~~To investigate if the air-filled porosity derived from the μCT images can explain the heterogeneity of label-derived emissions between the peat cores and injections, we tested if the average air-filled porosity above the injection depth was correlated to (i) the fractions of the label emitted as or (ii) the time until half of all emissions had occurred ($t_{1/2}$). This analysis was done separately for each injection depth.~~ We found no correlation between between air-filled porosity and the amount of label-derived CO_2 emitted after injections, but greater air-filled porosity was associated with more rapid emissions of $^{13}CO_2$ (lower $t_{1/2}$) at all injection depths (Fig. ~~9).~~ 10). We also tested for correlations between these measures ~~of~~ and pore network metrics (Fig. ~~Snn~~ S2). Again, we found no correlation between the analysed metrics and the fraction of the label emitted as CO_2. The slower release of $^{13}CO_2$ (~~higehr~~ higher $t_{1/2}$) ~~were~~ was associated with greater clustering coefficients (~~8cm~~ 8 cm depth) and betweenness centrality (all depths). These metrics, however, were themselves associated with lower air-filled porosity (Table ~~Snn~~ S1), such that we could not distinguish ~~if~~ statistically if the differences in $t_{1/2}$ ~~resulted~~ were driven by ~~from~~ air-filled porosity ~~*per se*~~ per se or the properties of the networks described by the network metrics. Clustering coefficients were negatively correlated with air-filled porosity unlike in previous studies (Kiuru et al., 2022a). Greater clustering coefficients, however, indicate a greater network connectivity, which would have the opposite effect on ~~release time (faster release in more connected networks with greater clustering coefficients)~~ the timing of $^{13}CO_2$ production. In contrast, higher air-filled porosity indicates ~~a that~~ that a greater part of the peat receives sufficient oxygen to convert the label to CO_2, and that such CO_2 can diffuse out of the peat column faster. It is therefore likely that air-filled porosity, not the clustering coefficient, was responsible for the observed correlations. Betweenness centrality indicates the probability that a given pore is part of the shortest ~~connnection~~ connection between pores at the top and bottom of the peat core. High betweenness centrality indicates that a small number of pores are essential for air transport through the peat cores, ~~an~~ and may therefore have contributed to a slower CO_2 release.

~~Overall, our results shows that pore network imaging at the rough resolution possible for intact peat cores of the size studied here (10cm) and at (near) native water content provided little additional information to what can be derived from macroscopic measures like injection depth, i.e., distance to surface, and air-filled porosity. Identifying the precise location of the injection in the pore networks might have provided additional information, but was not possible as the wooden injection position markers used in our study were not clearly visible in μCT images .~~

5 Conclusions

We have established an experimental setup to identify biogeochemical heterogeneity of micro-environments within peat cores that are involved in the production of CO_2 and CH_4 by combining laboratory-scale manipulation experiments and thorough μCT imaging of relatively large peat cores. μCT imaging has been used to study the physical heterogeneity before, but to our best knowledge this was the first attempt ~~to investigate~~ to directly demonstrate the spatial heterogeneity in (potential) biogeochemical transformation rates ~~and gas transport~~ through microinjections and monitoring of gas emissions at the peat
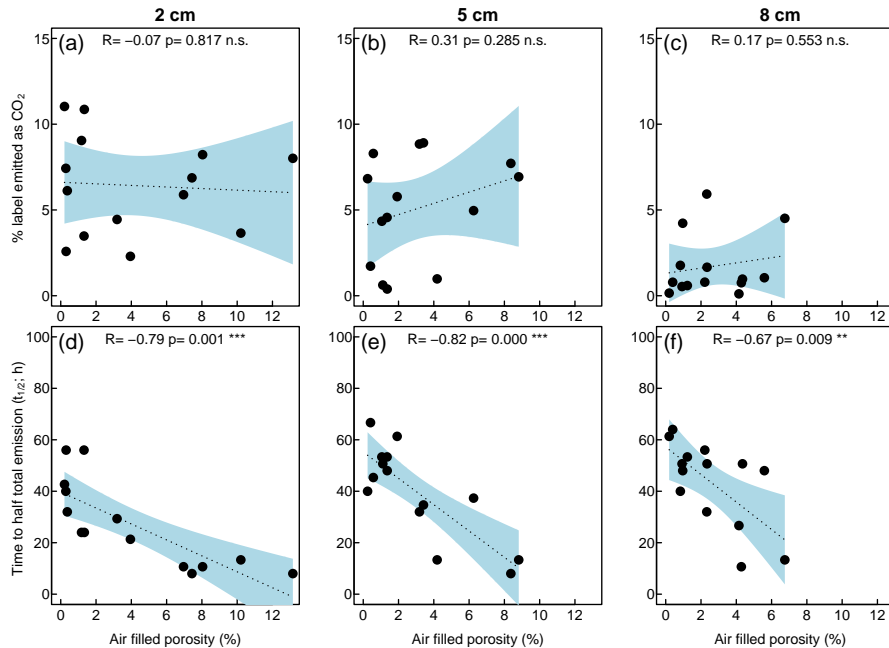
Figure 10. Correlations between μCT-derived air-filled porosity measured from the μCT images and the percentage of the label that has been emitted as $^{13}CO_2$ after injections at depths of 2 cm (a), 5 cm (b) and 8 cm (c). Further, correlation between air-filled porosity and the time until half of such emission rate had occurred after injections at depths of 2 cm (d), 5 cm (e) and 8 cm (f).

surface. Our approach is complementary to other recently applied methods, which use microscale measurements by μCT and microsensors to infer soil properties that are then used to explain macroscale properties. In contrast, our approach with locally

540 injected isotope-labeled substrates can help to elucidate distinct biogeochemical transformations similar to zygometric imaging but allowing repeated measurements although at lower spatial resolution. The highly variable responses to label injections found in our study demonstrate a high ~~heterogeneity of these processes~~ biogeochemical heterogeneity at the centimeter scale.

~~Our study~~ Our experiments also highlights the significant challenges associated with such ~~an undertaking~~a pursuit. The analysis of pore network by μCT imaging, which allowed us to study pore network architecture at the scale of fractions

545 of millimeters could not remove the remaining uncertainties in what governs the spatial heterogeneity in biogeochemical transformations.

Nevertheless, our study showed that the biogeochemical heterogeneity observed at a scale of centimeters (injection depths) to tens of centimeters (replicate peat cores from the same pit) was as large as the heterogeneity observed ~~at 10s~~ over tens of meters (between pits). Our work thus emphasizes that defining the relevant scale for the investigated processes is of key

550 importance for future studies.

Code and data availability. The Python scripts used in the μCT image processing and calculations are available at GitHub (https://github.com/pjkiuru/netw The μCT image and binary image data are available from the authors upon reasonable request. Raw data of the labelling experiment and the code used to process them is available at Zenodo (doi:10.5281/zenodo.11088028).

Author contributions. LK, AM, MP, and MR conceptualized the experiment. LK, AM, and MP collected samples in the field. LK conducted
555 the manipulative experiment. LK processed CO_2 and CH_4 emission data, PK processed and analysed μCT images. LK conducted the formal analysis. LK and AL wrote the first draft of the manuscript, which was revised based on input from all co-authors.

Competing interests. The authors declare no competing interests.

Acknowledgements. We thank Tatu Polvinen help constructing the measurement system.

Financial Support: This research has been supported by the Academy of Finland (grant nos. 325168, 325169, 339489, and 354501).
560 Annamari Laurén was supported by funding from the Academy of Finland to strengthen university research profiles in Finland for the years 2017–2021 (funding decision 311925). Maarit Raivonen was supported by SRC at the Academy of Finland (SOMPA, no. 312932) and EU Horizon 2020 (VERIFY, no. 776810). This work used services of the Helsinki University X-Ray Micro-CT Laboratory, also funded by the Helsinki Institute of Life Science (HiLIFE) under the HAIP platform.

References

Ball, B.: Modelling of soil pores as tubes using gas permeabilities, gas diffusivities, and water release, Journal of Soil Science, 32, 465–481, https://doi.org/10.1111/j.1365-2389.1981.tb01723.x, 1981.

Ballard, T. M.: Gaseous Diffusion Evaluation in Forest Humus, Soil Science Society of America Journal, 34, 532–533, https://doi.org/10.2136/SSSAJ1970.03615995003400030046X, 1970.

Bartholomeus, R. P., Witte, J. P. M., van Bodegom, P. M., van Dam, J. C., and Aerts, R.: Critical soil conditions for oxygen stress to plant roots: Substituting the Feddes-function by a process-based model, Journal of Hydrology, 360, 147–165, https://doi.org/10.1016/J.JHYDROL.2008.07.029, 2008.

Boon, A., Robinson, J. S., Nightingale, P. D., Cardenas, L., Chadwick, D. R., and Verhoef, A.: Determination of the gas diffusion coefficient of a peat grassland soil, European Journal of Soil Science, 64, 681–687, https://onlinelibrary.wiley.com/doi/full/10.1111/ejss.12056https://onlinelibrary.wiley.com/doi/abs/10.1111/ejss.12056https://bsssjournals.onlinelibrary.wiley.com/doi/10.1111/ejss.12056, 2013.

Bratbak, G. and Dundas, I.: Bacterial Dry Matter Content and Biomass Estimations, APPLIED AND ENVIRONMENTAL MICROBIOLOGY, 48, 755–757, 1984.

Chen, K., He, X., Liang, F., and Sheng, D.: Influences of ink-bottle effect evolution on water retention hysteresis of unsaturated soils: An experimental investigation, Engineering Geology, 330, 107 409, https://doi.org/10.1016/J.ENGGEO.2024.107409, 2024.

Du, Y., Guo, S., Wang, R., Song, X., and Ju, X.: Soil pore structure mediates the effects of soil oxygen on the dynamics of greenhouse gases during wetting–drying phases, Science of The Total Environment, 895, 165 192, https://doi.org/10.1016/J.SCITOTENV.2023.165192, 2023.

Elkhoury, J. E., Shankar, R., and Ramakrishnan, T. S.: Resolution and Limitations of X-Ray Micro-CT with Applications to Sandstones and Limestones, Transport in Porous Media, 129, 413–425, https://doi.org/10.1007/s11242-019-01275-1, 2019.

Fan, Z., Neff, J. C., Waldrop, M. P., Ballantyne, A. P., and Turetsky, M. R.: Transport of oxygen in soil pore-water systems: implications for modeling emissions of carbon dioxide and methane from peatlands, Biogeochemistry, 121, 455–470, https://doi.org/10.1007/S10533-014-0012-0/FIGURES/5, 2014.

Frolking, S., Talbot, J., Jones, M. C., Treat, C. C., Kauffman, J. B., Tuittila, E. S., and Roulet, N.: Peatlands in the Earth's 21st century climate system, https://doi.org/10.1139/a11-014, 19, 371–396, https://doi.org/10.1139/A11-014, 2011.

Gorham, E.: Northern Peatlands: Role in the Carbon Cycle and Probable Responses to Climatic Warming, Ecological Applications, 1, 182–195, https://doi.org/10.2307/1941811, 1991.

Gostick, J., Aghighi, M., Hinebaugh, J., Tranter, T., Hoeh, M. A., Day, H., Spellacy, B., Sharqawy, M. H., Bazylak, A., Burns, A., Lehnert, W., and Putz, A.: OpenPNM: A Pore Network Modeling Package, Computing in Science and Engineering, 18, 60–74, https://doi.org/10.1109/MCSE.2016.49, 2016.

Gostick, J. T.: Versatile and efficient pore network extraction method using marker-based watershed segmentation, Physical Review E, 96, 023 307, https://doi.org/10.1103/PHYSREVE.96.023307/FIGURES/13/MEDIUM, 2017.

Gostick, J. T., Khan, Z. A., Tranter, T. G., Kok, M. D., Agnaou, M., Sadeghi, M., and Jervis, R.: PoreSpy: A Python Toolkit for Quantitative Analysis of Porous Media Images, Journal of Open Source Software, 4, 1296, https://doi.org/10.21105/JOSS.01296, 2019.

Hagedorn, G., Mietchen, D., Morris, R., Agosti, D., Penev, L., Berendsohn, W., and Hobern, D.: Creative Commons licenses and the non-commercial condition: Implications for the re-use of biodiversity information, ZooKeys, 150, 127, https://doi.org/10.3897/zookeys.150.2189, 2011.

Hamamoto, S., Dissanayaka, S. H., Kawamoto, K., Nagata, O., Komtatsu, T., and Moldrup, P.: Transport properties and pore-network structure in variably-saturated Sphagnum peat soil, European Journal of Soil Science, 67, 121–131, https://doi.org/10.1111/EJSS.12312, 2016.

Higo, Y. and Kido, R.: A microscopic interpretation of hysteresis in the water retention curve of sand, Geotechnique, https://doi.org/10.1680/JGEOT.23.00084/ASSET/IMAGES/SMALL/JGEOT.23.00084-F8.GIF, 2023.

Hökkä, D. H., PhD, D. M. P., Stenberg, D. L., Heikkinen, P. J., and Laurén, P. A.: Changing role of water table and weather conditions in diameter growth of Scots pine on drained peatlands, https://doi.org/10.1139/cjfr-2024-0011, https://doi.org/10.1139/CJFR-2024-0011, 2024.

Jokinen, P., Pirinen, P., Kaukoranta, J.-P., Kangas, A., Alenius, P., Eriksson, P., Johansson, M., and Wilkman, S.: Climatological and oceanographic statistics of Finland 1991–2020, Tech. rep., Finnish Meteorological Institute, https://doi.org/10.35614/ISBN.9789523361485, 2021.

Keiluweit, M., Gee, K., Denney, A., and Fendorf, S.: Anoxic microsites in upland soils dominantly controlled by clay content, Soil Biology and Biochemistry, 118, 42–50, https://doi.org/10.1016/J.SOILBIO.2017.12.002, 2018.

Kettridge, N. and Binley, A.: Characterization of peat structure using X-ray computed tomography and its control on the ebullition of biogenic gas bubbles, Journal of Geophysical Research: Biogeosciences, 116, 1024, https://doi.org/10.1029/2010JG001478, 2011.

Kim, K., Kutlu, T., Kravchenko, A., and Guber, A.: Dynamics of N2O in vicinity of plant residues: a microsensor approach, Plant and Soil, 462, 331–347, https://doi.org/10.1007/S11104-021-04871-7/TABLES/1, 2021.

Kim, K., Gil, J., Ostrom, N. E., Gandhi, H., Oerther, M. S., Kuzyakov, Y., Guber, A. K., and Kravchenko, A. N.: Soil pore architecture and rhizosphere legacy define N2O production in root detritusphere, Soil Biology and Biochemistry, 166, 108 565, https://doi.org/10.1016/J.SOILBIO.2022.108565, 2022.

King, J. A. and Smith, K. A.: Gaseous diffusion through peat, Journal of Soil Science, 38, 173–177, https://doi.org/10.1111/j.1365-2389.1987.tb02134.x, 1987.

Kiuru, P., Palviainen, M., Grönholm, T., Raivonen, M., Kohl, L., Gauci, V., Urzainki, I., and Laurén, A.: Peat macropore networks-new insights into episodic and hotspot methane emission, Biogeosciences, 19, 1959–1977, https://doi.org/10.5194/bg-19-1959-2022, 2022a.

Kiuru, P., Palviainen, M., Marchionne, A., Grönholm, T., and Raivonen, M.: Pore network modeling as a new tool for determining gas diffusivity in peat, Biogeosciences, 19, 5041–5058, https://doi.org/https://doi.org/10.5194/bg-19-5041-2022, 2022b.

Korkiakoski, M., Ojanen, P., Penttilä, T., Minkkinen, K., Sarkkola, S., Rainne, J., Laurila, T., and Lohila, A.: Impact of partial harvest on CH4 and N2O balances of a drained boreal peatland forest, Agricultural and Forest Meteorology, 295, 108 168, https://doi.org/10.1016/J.AGRFORMET.2020.108168, 2020.

Kravchenko, A. N., Toosi, E. R., Guber, A. K., Ostrom, N. E., Yu, J., Azeem, K., Rivers, M. L., and Robertson, G. P.: Hotspots of soil N2O emission enhanced through water absorption by plant residue, Nature Geoscience 2017 10:7, 10, 496–500, https://doi.org/10.1038/ngeo2963, 2017.

Laine, J. and Vasander, H.: Ecology and vegetation gradients of peatlands, in: Peatlands in Finland, edited by Vasander, H., pp. 10–19, Finnish Peatland Society, Jyvaskyla, 1996.

Lauren, A.: Hydraulic, thermal and aeration properties of mor layers in Finland, Ph.D. thesis, University of Joensuu, 1999.

Laurén, A. and Mannerkoski, H.: Hydraulic Properties of Mor Layers in Finland, Scandinavian Journal of Forest Research, 16, 429–441, https://doi.org/10.1080/02827580152632829, 2001.

Leifeld, J., Wüst-Galley, C., and Page, S.: Intact and managed peatland soils as a source and sink of GHGs from 1850 to 2100, Nature Climate Change 2019 9:12, 9, 945–947, https://doi.org/10.1038/s41558-019-0615-5, 2019.

640   Limpens, J., Berendse, F., Blodau, C., Canadell, J. G., Freeman, C., Holden, J., Roulet, N., Rydin, H., and Schaepman-Strub, G.: Peatlands and the carbon cycle: From local processes to global implications - A synthesis, Biogeosciences, 5, 1475–1491, https://doi.org/10.5194/BG-5-1475-2008, 2008.

Mady, A. Y. and Shein, E. V.: Assessment of pore space changes during drying and wetting cycles in hysteresis of soil water retention curve in Russia using X-ray computed tomography, Geoderma Regional, 21, e00 259, https://doi.org/10.1016/J.GEODRS.2020.E00259, 2020.

645   McCarter, C. P., Rezanezhad, F., Quinton, W. L., Gharedaghloo, B., Lennartz, B., Price, J., Connon, R., and Van Cappellen, P.: Pore-scale controls on hydrological and geochemical processes in peat: Implications on interacting processes, Earth-Science Reviews, 207, 103 227, https://doi.org/10.1016/J.EARSCIREV.2020.103227, 2020.

Minkkinen, K. and Laine, J.: Effect of forest drainage on the peat bulk density of pine mires in Finland, Canadian Journal of Forest Research, 28, 178–186, https://doi.org/10.1139/x97-206, 1998.

650   Mualem, Y.: A conceptual model of hysteresis, Water Resources Research, 10, 514–520, https://doi.org/10.1029/WR010I003P00514, 1974.

Newman, M. E.: The Structure and Function of Complex Networks, https://doi.org/10.1137/S003614450342480, 45, 167–256, https://doi.org/10.1137/S003614450342480, 2006.

Ortega-Ramírez, P., Pot, V., Laville, P., Schlüter, S., Amor-Quiroz, D. A., Hadjar, D., Mazurier, A., Lacoste, M., Caurel, C., Pouteau, V., Chenu, C., Basile-Doelsch, I., Henault, C., and Garnier, P.: Pore distances of particulate organic matter predict N2O emissions from intact 655   soil at moist conditions, Geoderma, 429, 116 224, https://doi.org/10.1016/J.GEODERMA.2022.116224, 2023.

Otsu, N.: THRESHOLD SELECTION METHOD FROM GRAY-LEVEL HISTOGRAMS., IEEE Trans Syst Man Cybern, SMC-9, 62–66, 1979.

Pan, G. f., Zheng, Y. x., Yuan, S. y., Sun, D. x., Buzzi, O., Jiang, G. l., and Liu, X. f.: Microstructural insight into the hysteretic water retention behavior of intact Mile expansive clay, Soils and Foundations, 64, 101 427, https://doi.org/10.1016/J.SANDF.2024.101427, 2024.

660   Pires, L. F., Auler, A. C., Roque, W. L., and Mooney, S. J.: X-ray microtomography analysis of soil pore structure dynamics under wetting and drying cycles, Geoderma, 362, 114 103, https://doi.org/10.1016/J.GEODERMA.2019.114103, 2020.

R Development Core Team: R: A Language and Environment for Statistical Computing, http://www.r-project.org, 2015.

Ramirez, J. A., Baird, A. J., and Coulthard, T. J.: The effect of pore structure on ebullition from peat, Journal of Geophysical Research: Biogeosciences, 121, 1646–1656, https://doi.org/10.1002/2015JG003289, 2016.

665   Rezanezhad, F., Price, J. S., Quinton, W. L., Lennartz, B., Milojevic, T., and Van Cappellen, P.: Structure of peat soils and implications for water storage, flow and solute transport: A review update for geochemists, Chemical Geology, 429, 75–84, 2016.

Rohe, L., Apelt, B., Vogel, H. J., Well, R., Wu, G. M., and Schlüter, S.: Denitrification in soil as a function of oxygen availability at the microscale, Biogeosciences, 18, 1185–1201, https://doi.org/10.5194/BG-18-1185-2021, 2021.

Schlüter, S., Henjes, S., Zawallich, J., Bergaust, L., Horn, M., Ippisch, O., Vogel, H. J., and Dörsch, P.: Denitrification 670   in soil aggregate analogues-effect of aggregate size and oxygen diffusion, Frontiers in Environmental Science, 6, 358 214, https://doi.org/10.3389/FENVS.2018.00017/BIBTEX, 2018.

Sihi, D., Davidson, E. A., Savage, K. E., and Liang, D.: Simultaneous numerical representation of soil microsite production and consumption of carbon dioxide, methane, and nitrous oxide using probability distribution functions, Global Change Biology, 26, 200–218, https://doi.org/10.1111/GCB.14855, 2020.

Stock, S. R.: Recent advances in X-ray microtomography applied to materials, International Materials Reviews, 53, 129–181, https://doi.org/10.1179/174328008X277803, 2008.

Van Der Walt, S., Schönberger, J. L., Nunez-Iglesias, J., Boulogne, F., Warner, J. D., Yager, N., Gouillart, E., and Yu, T.: Scikit-image: Image processing in python, PeerJ, 2014, e453, https://doi.org/10.7717/PEERJ.453/FIG-5, 2014.

Vidal-Beaudet, L. and Charpentier, S.: Percolation Theory and Hydrodynamics of Soil-Peat Mixtures, Soil Science Society of America Journal, 64, 827–835, https://doi.org/10.2136/SSSAJ2000.643827X, 2000.

Virtanen, P., Gommers, R., Oliphant, T. E., Haberland, M., Reddy, T., Cournapeau, D., Burovski, E., Peterson, P., Weckesser, W., Bright, J., van der Walt, S. J., Brett, M., Wilson, J., Millman, K. J., Mayorov, N., Nelson, A. R., Jones, E., Kern, R., Larson, E., Carey, C. J., Polat, I., Feng, Y., Moore, E. W., VanderPlas, J., Laxalde, D., Perktold, J., Cimrman, R., Henriksen, I., Quintero, E. A., Harris, C. R., Archibald, A. M., Ribeiro, A. H., Pedregosa, F., van Mulbregt, P., Vijaykumar, A., Bardelli, A. P., Rothberg, A., Hilboll, A., Kloeckner, A., Scopatz, A., Lee, A., Rokem, A., Woods, C. N., Fulton, C., Masson, C., Häggström, C., Fitzgerald, C., Nicholson, D. A., Hagen, D. R., Pasechnik, D. V., Olivetti, E., Martin, E., Wieser, E., Silva, F., Lenders, F., Wilhelm, F., Young, G., Price, G. A., Ingold, G. L., Allen, G. E., Lee, G. R., Audren, H., Probst, I., Dietrich, J. P., Silterra, J., Webber, J. T., Slavič, J., Nothman, J., Buchner, J., Kulick, J., Schönberger, J. L., de Miranda Cardoso, J. V., Reimer, J., Harrington, J., Rodríguez, J. L. C., Nunez-Iglesias, J., Kuczynski, J., Tritz, K., Thoma, M., Newville, M., Kümmerer, M., Bolingbroke, M., Tartre, M., Pak, M., Smith, N. J., Nowaczyk, N., Shebanov, N., Pavlyk, O., Brodtkorb, P. A., Lee, P., McGibbon, R. T., Feldbauer, R., Lewis, S., Tygier, S., Sievert, S., Vigna, S., Peterson, S., More, S., Pudlik, T., Oshima, T., Pingel, T. J., Robitaille, T. P., Spura, T., Jones, T. R., Cera, T., Leslie, T., Zito, T., Krauss, T., Upadhyay, U., Halchenko, Y. O., and Vázquez-Baeza, Y.: SciPy 1.0: fundamental algorithms for scientific computing in Python, Nature Methods 2020 17:3, 17, 261–272, https://doi.org/10.1038/s41592-019-0686-2, 2020.

Wachinger, G., Fiedler, S., Zepp, K., Gattinger, A., Sommer, M., and Roth, K.: Variability of soil methane production on the microscale: spatial association with hot spots of organic material and Archaeal populations, Soil Biology and Biochemistry, 32, 1121–1130, https://doi.org/10.1016/S0038-0717(00)00024-9, 2000.

Wright, W., Ramirez, J. A., and Comas, X.: Methane Ebullition From Subtropical Peat: Testing an Ebullition Model Reveals the Importance of Pore Structure, Geophysical Research Letters, 45, 6992–6999, https://doi.org/10.1029/2018GL077352, 2018.

Xu, X., Yuan, F., Hanson, P. J., Wullschleger, S. D., Thornton, P. E., Riley, W. J., Song, X., Graham, D. E., Song, C., and Tian, H.: Reviews and syntheses: Four decades of modeling methane cycling in terrestrial ecosystems, Biogeosciences, 13, 3735–3755, https://doi.org/10.5194/bg-13-3735-2016, 2016.

Yu, Z., Peng, P., Sheng, G., and Fu, J.: Determination of hexabromocyclododecane diastereoisomers in air and soil by liquid chromatography-electrospray tandem mass spectrometry., Journal of chromatography. A, 1190, 74–79, https://doi.org/10.1016/j.chroma.2008.02.082, 2008.